

SLL 81 392

ACCELERATION OF PROJECTILES
TO HYPERVELOCITIES USING A
SERIES OF IMPLoded ANNULAR
PLASMA DISCHARGES

DISTRIBUTION STATEMENT

Approved for public release
Distribution Unlimited

JAYCOR

DTIC QUALITY INSURED

PLEASE RETURN TO:

BMD TECHNICAL INFORMATION CENTER
BALLISTIC MISSILE DEFENSE ORGANIZATION
7100 DEFENSE PENTAGON
WASHINGTON D.C. 20307-5100

19980309 376

Accession Number: 3808

Publication Date: Oct 01, 1979

Title: Acceleration of Projectiles to Hypervelocities Using a Series of Imploded Annular Plasma Discharges

Personal Author: Tidman, D.A.; Goldstein, S.A.

Corporate Author Or Publisher: JAYCOR, 205 South Whiting Street, Alexandria, VA 22304 Report Number: JAYCOR Tech Note 350-79-011

Comments on Document: Archive, RRI, DEW. Communicated to Journal of Applied Physics

Descriptors, Keywords: Directed Energy Weapon DEW Acceleration Projectile Hypervelocity Series Implode Annular Plasma Discharge Theory Device Material Impact Space Probe Launch Fusion Z-pinch

Pages: 37

Cataloged Date: Oct 19, 1992

Document Type: HC

Number of Copies In Library: 000001

Record ID: 24987

Source of Document: DEW

ACCELERATION OF PROJECTILES
TO HYPERVELOCITIES USING A
SERIES OF IMPOSED ANNULAR
PLASMA DISCHARGES

D. A. Tidman and S. A. Goldstein

JAYCOR Tech Note 350-79-011

JAYCOR
205 South Whiting Street
Alexandria, VA. 22304

and

Institute for Physical Science and Technology
University of Maryland
College Park, MD. 20742

October, 1979

(Communicated to the Journal of Applied Physics)

ABSTRACT

A mass accelerator system using a series of imploded annular plasma pinches to propel projectiles of mass ranging from grams to kilograms up to high velocities is analyzed theoretically. Such a device would have applications ranging from basic materials and impact studies to space probe launching and impact fusion.

I. INTRODUCTION

The implosion dynamics of self z-pinch annular discharges is a subject that has been well studied in the context of such devices as the plasma focus¹, or dynamically imploded annular foils² or gas puffs for radiation sources. In this paper we give some analysis of a recently proposed concept³ for a mass accelerator system using a series of imploded discharges (MAID), which are axially aligned and imploded sequentially on to the surface of a suitably tapered projectile in order to propel it. The system appears capable of accelerating projectiles of mass ranging from grams to kilograms up to velocities well above 10^6 cm/sec and possibly as high as 10^7 cm/sec. It is also expected to have good projectile survival and stability properties, could have a high repetition rate, and the attainable accelerations appear to be limited principally by the requirement that the projectile should not undergo material damage such as crushing or spalling. The potential applications which would motivate the development of this technology include basic materials and impact studies, the launching of small space probes, or possibly impact fusion.

The basic accelerator module is shown in Figure 1. It consists of an anode and cathode which for example could be discs with a hole at the center of sufficient radius to allow passage of the projectile. At a suitable time interval before arrival of the projectile in the anode-cathode gap from the left in Figure 1, a high voltage pulse is switched on across the electrodes which is sufficient to initiate a discharge through flashover in the low density gas along the inner surface of the insulator which separates the electrodes. This high current annular discharge is then driven by its azimuthal magnetic field radially inward away from the insulator surface and accelerates towards the axis of the module. As the discharge advances

radially inward, it accumulates and compresses more plasma by sweeping up the background gas via the snow plow effect, so that the velocity and mass of gas colliding with the projectile surface depends on the initial background gas pressure (for example ~ 10 torr) and module size. The inner edge of the insulator between the anode and cathode could also be slightly tapered as shown, so that the imploding annular plasma becomes itself more tapered during its implosion so as to match the projectile surface, although this tapering is not necessary and the insulator could also be a simple straight cylindrical section separating the anode and cathode. The discharge is timed so that it collides with the projectile surface when its front edge is approximately aligned with the cathode. The projectile is propelled both by the imploded discharge momentum and pressure, and by reaction to its ablated surface material.

Figure 2 shows a mass accelerator consisting of a series of axially aligned discharge modules. The voltages of each module would be typically kilovolts to ten kilovolts depending on the application. As the projectile is propelled forward from one anode-cathode gap into the next module, a sensing device (for example the interruption of a light beam) is used to determine when to trigger the next diode modules. This is timed so that the next discharge arrives at the projectile surface when it is appropriately positioned in the anode-cathode gap for further acceleration, and the sequence is repeated as the projectile advances axially along the accelerator. Note that for devices that take full advantage of the power compression that results if the radius to the inner edge of the insulator is much larger than the projectile radius, several discharges ahead of the projectile could be initiated and be in different stages of implosion at any one time.

Some advantages of this system are (i) the implosions effectively focus the discharge gas momentum onto the projectile where the maximum pressures in the system then result, (ii) power compression (discussed in Section 2), (iii) the expected good survivability properties of either metallic or insulator projectiles propelled to high velocities by gas pressure instead of by eddy-current inducing magnetic fields, and (iv) frictional contact with confining walls as occurs in rail guns is avoided, so that the system has a high potential repetition rate.

As an example of the approximate scaling involved, assume that the projectile has a mass of M grams and is accelerated up to a velocity of U cm/sec with an average acceleration of \dot{U} cm/sec² (averaged over a module plus gap between modules). The average total power in the electrical energy pulse that is required to generate this acceleration is then

$$P = nP_{\text{mod}} = 10^{-7} MU \dot{U} / \epsilon \text{ watts,} \quad (1)$$

where ϵ is the overall efficiency with which electrical energy is transferred from the electrical storage system to projectile kinetic energy. In this formula we distinguish between P and the power P_{mod} of each module, where n is the average number of discharge modules that are operating at any one time with their plasmas in various stages of implosion timed to impact the projectile surface as it passes through. This power would produce a projectile with final kinetic energy.

$$5.10^4 M \left(\frac{U_f}{10^6} \right)^2 \text{ Joules}$$

if applied for an acceleration length $L = U_f^2 / 2\dot{U}$ for the case in which the acceleration \dot{U} is constant. For example, assuming $\dot{U} = 5.10^8$ cm/sec²,

$\epsilon = 0.1$, $U_f = 3 \cdot 10^6$ cm/sec gives for the final maximum power $P_{\text{mod}} = 1.5 \cdot 10^9$ M/n watts per module, and a projectile energy of $4.5 \cdot 10^5$ M Joules acquired in an accelerator length of 100 meters.

More generally the efficiency in (1) (and acceleration) are not constant along the accelerator. Further, ϵ is made up of two parts,

$$\epsilon = \epsilon_{\text{impl}} \epsilon_{\text{prop}} \quad , \quad (2)$$

where ϵ_{impl} is the efficiency with which electrical energy is transferred to the imploding plasma shells, and ϵ_{prop} is the propulsion efficiency with which this energy is in turn transmitted to projectile kinetic energy. These efficiencies are functions of various parameters characterizing the modules and the projectile, and will be discussed in Sections II and III.

The projectiles (Figure 3) could be constructed out of various materials. For cases in which high currents are used, it is important to minimize heating inside the projectile (if it is electrically conducting) which can arise from eddy currents in its outer layers due to penetration of the surface magnetic fields through the discharge plasma into the solid projectile, since this can cause premature melting of the projectile before a high velocity is reached. This problem is alleviated for metallic projectiles by arranging that the plasma pressure on the projectile derive mainly from the implosion energy of the discharge so that the magnetic fields remain small at the inner plasma edge during impact with the projectile surface (the driving current could in fact be zero at impact as discussed in Section 2D, which also appears desirable for projectile stability, Section IV). Eddy current heating can also be eliminated for cases in which lower accelerations (weaker projectiles) are acceptable by constructing the

projectile of insulator material. In this situation, current is then able to flow only through the surface plasma layer pinched against the projectile, so that Joule dissipation is zero inside the projectile except for the thin-conducting skin layer that has been converted to plasma at its outer edge. This plasma layer advances into the projectile relatively slowly via thermal conduction and ablation during the acceleration, i.e., more slowly than would be the case for the more deeply penetrating skin current layer that occurs for metallic projectiles in devices in which magnetic fields provide the primary propulsion instead of plasma momentum and reaction forces as in this device.

II. IMPLOSION RELATIONS

The implosion speed V_{impl} of the annular discharge as it approaches the projectile surface must satisfy $V_{\text{impl}} > U \tan \theta$, where U is the projectile velocity and θ its cone half-angle. Under these circumstances the timing can be arranged so that contact is not made between the discharge and any part of the tapered projectile prior to arrival of the projectile in the gap, and further, the discharge can be timed to collide with at least some of the projectile surface before the projectile has had time to move ahead of the electrode gap. We also note that the implosion time,

$$\tau_{\text{impl}} = \int_{a_p}^{a_w} \frac{da}{V_{\text{impl}}(a)}, \quad (3)$$

for the plasma to implode radially from the insulator surface to the projectile surface, can be larger than the transit time of approximately ℓ/U taken for the projectile to cross the electrode gap, where the inwardly directed radial velocity of the annular discharge, $V_{\text{impl}} = |\dot{a}|$, is a function of its radial position a , a_w is the radius of the insulator surface, a_p the radius

of the projectile at a point located at a distance $\sim \ell/2$ back from the leading edge of the tapered section of the projectile, and ℓ the axial length of the discharge as shown in Figure 1. For cases in which this condition is satisfied some power multiplication can be obtained in that the driving voltage and current can be applied so that the discharge plasma accumulates implosion momentum for a time longer than the encounter time available to communicate this accumulated momentum to the projectile. It is also important that the gas density in which the discharge is initiated be sufficiently low that the final implosion velocity exceeds the projectile velocity, while at the same time sufficiently high for the implosion radius involved that the discharge momentum provides a high surface pressure on impact with the projectile. Analysis of these requirements involves solving hydrodynamic and circuit equations for magnetically imploded plasma shells. We next give a simple generalization of a model by Mosher² for the case of interest to us, namely that in which snow plowing of ambient gas occurs.

A. Approximate Implosion Model.

The equations of motion for a cylindrically symmetric gas implosion in a module of radius a_w and gap length ℓ can be written

$$\frac{\partial P}{\partial t} = - 2\pi\ell \int_0^{a_w} dr \, r \left[\frac{1}{c} jB + \frac{\partial p}{\partial r} \right] , \quad (4)$$

where

$$P = 2\pi\ell \int_0^{a_w} r \, dr \, \rho V_r \quad (5)$$

is the integrated radial momentum, V_r the fluid velocity,

$$p = nT (1 + Z) \quad (6)$$

the gas pressure,

$$j = \frac{c}{4\pi} \frac{1}{r} \frac{\partial}{\partial r} (rB) \quad (7)$$

the current density, B the azimuthal pinch magnetic field, and

$$I = \int_0^{a_w} 2\pi r dr j \quad (8)$$

is the total plasma current.

If we assume a snow plow model in which all the gas of initial uniform density ρ_0 is swept up by the implosion, then $P \approx \pi \rho_0 \ell (a_w^2 - a^2) \dot{a}$. Further, assuming the annular shell thickness Δa is small compared with a (this breaks down near the end of the implosion and is discussed in Section 2F), the coupled system of imploding plasma and circuit equations become

$$m_g \frac{d}{dt} \left[\left(1 - \frac{a^2}{a_w^2} \right) \dot{a} \right] = - \frac{I^2 \ell}{ac^2} \quad , \quad (9)$$

$$V = \frac{Q}{C} = \frac{d}{dt} (LI) + IR, \quad I = - \dot{Q} \quad (10)$$

$$L = L_g + \frac{2\ell}{c^2} \ln \left(\frac{a_w}{a} \right) \quad , \quad (11)$$

$$R \approx \ell / 2\pi \sigma a \delta \quad , \quad (12)$$

for an implosion driven by discharge of a capacitor C, where L, L_g , R, V are the total inductance, inductance external to the module, discharge resistance, and voltage, and

$$m_g = \pi a_w^2 \ell \rho_0 \quad (13)$$

is the mass of gas in the module. In the formula for the discharge resistance we take δ as the current penetration skin depth,

$$\delta = \left(\frac{c^2 t}{4\pi\sigma} \right)^{1/2} + \delta_{\text{flash}} \quad , \quad (14)$$

where σ is assumed constant and δ_{flash} is the small initial conducting layer thickness associated with the initiating surface breakdown at a_w .

B. Efficiency of Implosion.

Multiplying (10) by I and integrating gives

$$\int_0^T dt VI = \int_0^T dt L^{-1} \frac{d}{dt} \left(\frac{1}{2} L^2 I^2 \right) + \int_0^T dt I^2 R \quad .$$

Using $I = -\dot{Q}$, $Q = CV$, $\dot{L} = -2\dot{a}\ell/ac^2$, and $B = 2I/ac$ with $I(t=0) = 0$, we find

$$\frac{1}{2}C(V_0^2 - V^2) = \frac{1}{2}LI^2 - \int_0^T dt \left(\frac{B^2}{8\pi} \right) 2\pi a \dot{a} \ell + \int_0^T dt I^2 R \quad , \quad (15)$$

which displays the partition of energy between the change in capacitor storage, inductive energy, kinetic energy of the implosion W_{imp} , and Joule dissipation.

The efficiency for transfer of electrical energy to implosion kinetic energy will be defined as

$$\epsilon_{\text{impl}} = \frac{W_{\text{impl}}}{(\frac{1}{2} CV_0^2)} \frac{1}{(1-f)} \equiv \frac{W_{\text{impl}}}{W_{\text{impl}} + \int_0^{t_{\text{impl}}} dt I^2 R + \frac{1}{2} L_0 I^2 (t_{\text{impl}})} \quad (16)$$

In this expression, f is the fraction of the original capacitor bank energy that remains stored in the capacitor at the end of the implosion, assuming a switch can be opened at that time so that the energy can be usefully preserved for later use. For example, the voltage may reverse prior to impact and recharge C with the opposite polarity. Note, if we drop the factor $(1-f)^{-1}$ in (16), then $W_{\text{impl}}/(\frac{1}{2} CV_0^2)$ is the fraction of stored energy transferred to a single implosion.

C. Dimensionless Equations.

It is useful in deriving scaling laws to write (9) and (10) in the dimensionless form

$$\frac{d}{d\tau} \left[(1 - A^2) \frac{dA}{d\tau} \right] = - \frac{i^2}{A} \quad , \quad (17)$$

$$\frac{d^2}{d\tau^2} (\mathcal{L}i) + \frac{d}{d\tau} \left(\frac{ir}{A(\tau^{\frac{1}{2}} + \epsilon)} \right) + i = 0 \quad , \quad (18)$$

where the dimensionless radius A , current i , and time τ are defined by

$$A = \frac{a}{a_w} \quad , \quad i = \frac{I}{I_0} \quad , \quad \tau = \omega t \quad , \quad (19)$$

and

$$\left\{ \begin{array}{l} \mathcal{L} = \frac{L}{L_0} = \left(1 - \frac{L_m}{L_g} \frac{\ln A}{\ln \left(\frac{a_w}{a_p} \right)} \right) / \left(1 + \frac{L_m}{L_g} \right) \\ L_0 = L_g + L_m, \quad L_m = \frac{2\ell}{c^2} \ln \left(\frac{a_w}{a_p} \right) \\ \omega = (L_0 C)^{-1/2} \\ I_0 = c a_w \omega (m_g / \ell)^{1/2} \\ r = \frac{2\ell}{c a_w L_0 (4\pi\sigma\omega)^{1/2}} \\ \frac{1}{\sigma} = \frac{Z \ln \Lambda}{1.7 \cdot 10^{14} T_{ev}^{3/2}} + \frac{1}{\sigma_{eo}} \end{array} \right. \quad (20)$$

where σ_{eo}^{-1} is the contribution to the resistivity from electron-neutral scattering.

The initial conditions at $\tau = 0$ are

$$\begin{aligned} A &= 1 - \frac{\delta_{flash}}{a_w} \approx 1, \quad i = 0, \quad \frac{dA}{d\tau} = 0, \\ \left(\frac{di}{d\tau} \right)_{\tau=0} &= \frac{V_0}{L_g I_0 \omega} = \frac{(2C\ell)^{1/2}}{a_w} \left(1 + \frac{L_m}{L_g} \right) \left\{ \frac{\frac{1}{2} C V_0^2}{\pi a_w^2 \rho_0 c^2 \ell} \right\}^{1/2} \end{aligned} \quad (21)$$

Solutions are insensitive to the initial thin flash-over layer δ_{flash} which appears in both the initial value of A and also in the initial resistance through the small quantity $\epsilon = \delta_{\text{flash}} (4\pi\sigma\omega/c^2)^{1/2}$ in Equation (18). We note that impact with the projectile of radius a_p occurs when $A = a_p/a_w$, at which point $\mathcal{L} = 1$ and the implosion energy is

$$W_{\text{impl}} = \frac{1}{2} m_g a_w^2 \omega^2 \left(\frac{dA}{d\tau} \right)_{\text{imp}}^2, \quad (22)$$

and the efficiency (16) can be written

$$\epsilon_{\text{impl}} = \frac{\left(\frac{dA}{d\tau} \right)_{\text{imp}}^2 \left(\frac{L_m}{L_g} \right) \left(1 + \frac{L_m}{L_g} \right)}{\left(\frac{di}{d\tau} \right)_0^2 2 (1-f) \ln \left(\frac{a_w}{a_p} \right)} \quad (23)$$

D. Numerical Examples.

From (17) - (21) we see that A and i are functions of the dimensionless parameters

$$\frac{L_m}{L_g}, \quad \frac{a_w}{a_p}, \quad r.$$

For given values of these, the initial value $(di/d\tau)_0$ can be found numerically for which $i = 0$ when impact occurs. For this particular case, which we choose for stability reasons (see Section IV), there is no inductively stored energy at impact and the capacitor becomes partially recharged with the opposite polarity. It is essentially the case for which the implosion time t_{impl} is of order the $\sqrt{L_0 C}$ time in most situations. Once we have numerical solutions to (17) and (18) for choices of the above parameters, we can invert (21) and use

$$\rho_0 = \frac{C^2 V_0^2}{\pi a_w^4 C^2} \left(1 + \frac{L_m}{L_g} \right)^2 \left(\frac{di}{d\tau} \right)_0^{-2}, \quad (24)$$

$$V_{impl} = a_w \omega \left(\frac{dA}{d\tau} \right)_{impl}, \quad (25)$$

$$\omega = \sqrt{\frac{1}{L_0 C}} \equiv \frac{\tau_{impl}}{t_{impl}}, \quad (26)$$

to obtain the gas density, implosion velocity, etc., for various systems.

In Figure 4, we have plotted the dimensionless impact velocity $(dA/d\tau)_{impl}$, implosion time τ_{impl} , and initial gradient $(di/d\tau)_0$ (for which $i_{impl} = 0$), as functions of the dimensionless resistance r for the two examples

$$\frac{L_m}{L_g} = 0.5, 1.0; \quad \frac{a_w}{a_p} = 10.$$

Using (23), the fraction of energy $(1-f)\epsilon_{impl}$ that is transferred to implosion kinetic energy in a single implosion is also plotted (f is the fraction restored to the capacitor bank and potentially recoverable at τ_{impl}).

Figure 5 shows the variation of dimensionless implosion radius A and current i for one of these cases in the zero resistance limit $r = 0$ (this would correspond to $\epsilon_{impl} = 1$).

We see from Figure 4 that the transfer efficiency can be very high, up to about 57% for the case in which the external circuit inductance L_g equals the maximum module inductance, L_m , and the resistance r is negligible.

As a specific example consider the class of systems for which $L_m/L_g = 1$, $a_w/a_p = 10$, $r \approx 0$. From the numerical results in Figure 4, and noting that the initially stored electrical energy is

$$W = \frac{1}{2} C V_0^2 ,$$

it then follows from (24) - (26) that

$$V_{impl} = \frac{1.1 \cdot 10^5 a_w V_{kv}}{(\ell W_{kJ})^{1/2}} \text{ cm/sec}$$

$$\rho_0 = \frac{0.29 W_{kJ}^2}{a_w^4 V_{kv}^2} \text{ gm/cm}^3$$

$$t_{impl} = 10^{-5} (\ell W_{kJ})^{1/2} / V_{kv} \text{ sec,}$$

where the initial voltage V_0 and stored energy W are in kilovolts and kilojoules as indicated by the subscripts. For example, if $a_w = 15$ cm, $\ell = 2$ cm, $V_0 = 2$ kV, $W = 5$ kJ, then $V_{impl} \approx 10^6$ cm/sec, $\rho_0 = 3.6 \cdot 10^{-5}$ gm/cm³, and $t_{impl} = 16$ μ sec. The general scaling is also clear from the above formulas. In order to achieve higher velocity implosions we must use higher driving voltages or larger radii modules (although an upper limit to the aspect ratio a_w/a_p will be set by the possible growth of instabilities in the imploding shell). Lower gas densities and shorter implosion times are then involved and a fuller survey of this scaling will be given later.

E. Plasma Temperature

In general an energy equation should be added to (9) - (12) to determine the electron temperature required in the conductivity, σ . However, for most systems the largest part of the impedance is inductive, so that Eqs. (9) - (12) are insensitive to T , although T does play an important role in the annular shell thickness as discussed in Section F.

An approximate energy equation for T can be obtained by first noting that the necessary condition for a coronal equilibrium plasma state is typically satisfied, i.e., $n_e \tau_{\text{impl}} > 10^{12}$, since $\tau_{\text{impl}} \sim 10^{-5}$ and the annular gas density, which is compressed over the ambient value, exceeds $10^{17}/\text{cm}^3$. Further the implosion time-integrated Joule dissipation exceeds the thermal energy content of the gas, so that an approximate balance between Joule heating and radiation prevails, i.e.,

$$I^2 R \approx \text{smaller of} \begin{cases} 2\pi a \ell \Delta a P_c \\ 4\pi a \ell \sigma_B T^4 \end{cases}, \quad (27)$$

where P_c is the coronal equilibrium emission and the second expression the black body emission.

Consider for example nitrogen (which becomes atomic in the discharge) as the driving gas. Breton et al⁴ give coronal equilibrium results for the total emission (including line, continuum, and dielectronic recombination) that can be fitted so that the above expressions become,

$$\begin{cases} 2\pi a \ell \Delta a 4 \cdot 10^7 P_{\text{torr}}^2 \bar{Z} (T_{\text{ev}} - 3.4), & \text{for } 4 \leq T_{\text{ev}} \leq 10 \\ 4\pi a \ell 10^5 T_{\text{ev}}^4 & \text{watts} \end{cases}$$

Now typical values for I^2R are $\sim 10^8$ watts, so T_{ev} is typically a few eV. Further, since P_{torr} increases due to compression to a final value that can be $\sim 10^2$, we see that black-body emission is approximately dominant for nitrogen. Thus for finite t ,

$$T \approx 3 \cdot 10^{-3} \left(\frac{I(\text{amps})}{a} \right)^{\frac{8}{19}} \left(\frac{\bar{Z} \ln \Lambda}{t} \right)^{\frac{2}{19}} \left(1 + \frac{\sigma_p}{\sigma_{eo}} \right)^{\frac{2}{19}} \text{ eV.}$$

Since $\bar{Z} \sim 1$, $t \sim 10^{-5}$ sec, and the plasma resistivity dominates neutral collisions, this results in a temperature which is clamped at about 2 eV.

F. Estimated Thickness of the Annular Plasma Shell.

In the above model the finite thickness Δa of the imploded plasma annulus is treated as small compared with a . This thickness determines the pressure pulse and characteristic time in which momentum is transmitted to the projectile, and a proper treatment of this structure necessitates use of a detailed computer model.

However, a rough estimate of the thickness Δa can be obtained by considering the simple case of a 1D layer of plasma propelled magnetically with a constant acceleration g . Assuming field diffuses into the swept up plasma slowly on a sound transit time across Δa , an approximate pressure balance prevails, i.e.,

$$\frac{\partial}{\partial x} \left\{ \frac{B^2}{8\pi} + nT(1+Z) \right\} = -n m_0 g, \quad (28)$$

from which the density profile follows as

$$n = - \frac{1}{8\pi T(1+Z)} \int_0^x dx' \frac{\partial B^2}{\partial x'} e^{\frac{g}{c_s^2}(x' - x)}$$

where

$$c_s = \left(\frac{T(1+Z)}{m_0} \right)^{1/2}$$

is the sound speed.

Various models for B can be chosen, such as a linear diffusion ramp $B = B_0(1 - x/\delta)$, $0 \leq x \leq \delta = (c^2 t / 4\pi\sigma)^{1/2}$. Essentially, the result is the profile shown in Figure 6 in which n increases from zero on the swept-up field-supported side to a maximum value in a skin depth δ , and then undergoes an exponential-atmosphere decrease with a scale length c_s^2/g . A characteristic thickness which includes these two regions is

$$\Delta a = \frac{c_s^2}{g} + \left(\frac{c^2 t}{4\pi\sigma} \right)^{1/2} \quad (29)$$

A crude estimate for the implosions we are concerned with then follows by substituting $g \approx V_{\text{impl}}^2 / 2a_w$ and $t \approx t_{\text{impl}}$ in (29). For example, a low density air implosion with $T = 2$ eV, $Z = 1$, $t_{\text{impl}} = 10^{-5}$ sec, $a_w = 15$ cm, $V_{\text{impl}} = 5 \cdot 10^6$ cm/sec, gives $\Delta a \approx 2$ cm. A point to note is that high temperature implosions should be avoided so that the exponential atmosphere does not extend inward too far ahead of the swept-up gas and thus into the path of the projectile (see Figure 6).

III. COUPLING OF IMPLOSION ENERGY TO PROPULSION OF THE PROJECTILE

In Figure 7 we show imploding plasma incident with velocity $(U^2 + V_{\text{impl}}^2)^{1/2}$ in the projectile rest frame, where U is the projectile axial velocity in the accelerator frame, V_{impl} the radial plasma velocity, and θ the projectile cone half angle along its impact section. After impact with the surface the plasma undergoes reflection (with reduced momentum and energy) at an angle between the two extremes of specular reflection (path 1) or normal reflection (path 2). Since the exact reflection vector depends on details of the coupling processes at the projectile (such as viscosity, radiation, and conduction in the boundary layer between the solid surface and the outgoing shock), we will confine our discussion to the above two limiting cases.

Consider a series of modules each of which impart a small velocity increment dU to a projectile of mass M by imploding a gas mass dm with velocity V_{impl} . The projectile energy gain and implosion energy are

$$\begin{aligned} dW_{\text{proj}} &= MU \, dU \\ dW_{\text{impl}} &= \frac{1}{2} dm \, V_{\text{impl}}^2 \end{aligned} \quad (30)$$

Now suppose the incoming plasma momentum is absorbed and that a mass of gas $(dm + dM)$ is "re-emitted" with a reduced velocity V_{emiss} at an average angle ϕ to the surface normal as shown in Figure 7. Momentum conservation then gives

$$MdU = dm \left\{ -U + \sqrt{\alpha} (U^2 + V_{\text{impl}}^2)^{1/2} \left[1 + \left(\frac{dM}{dm} \right)_{\text{abl}} \right]^{1/2} \sin(\theta + \phi) \right\}, \quad (31)$$

where we have allowed for loss of a fraction $(1 - \alpha)$ of the implosion kinetic energy to sinks such as radiation, ablation, and internal motion of the projectile, and the extra mass dM re-emitted is due to ablation, i.e., the plasma re-emission velocity was determined by

$$\alpha \frac{1}{2} dm (U^2 + V_{imp1}^2) = \frac{1}{2} (dm + dM) V_{emiss}^2$$

Note, $(dM/dm)_{abl} < 1$ corresponds to a mainly implosion momentum drive, and $(dM/dm)_{abl} > 1$ to a mainly rocket reaction drive in which the implosion provides energy but not much momentum. The average "re-emission" angle ϕ lies between two limiting extremes:

$$\phi = \frac{\pi}{2} - \psi + \theta, \text{ specular case 1,}$$

$$\phi = 0, \text{ normal emission case 2.}$$

The propulsion energy efficiency can now be written

$$\epsilon_{prop} = \frac{dW_{proj}}{dW_{imp1}} = 2 \{-x^2 + \beta x (1 + x^2)^{\frac{1}{2}}\}, \quad (32)$$

where for the two limiting cases

$$\begin{aligned} \beta &= \sqrt{\alpha} \left[1 + \left(\frac{dM}{dm} \right)_{abl} \right]^{\frac{1}{2}} \cos(\psi - 2\theta), \text{ case 1,} \\ \beta &= \sqrt{\alpha} \left[1 + \left(\frac{dM}{dm} \right)_{abl} \right]^{\frac{1}{2}} \sin\theta, \text{ case 2,} \end{aligned} \quad (33)$$

and

$$x = \frac{U}{V_{imp1}}, \tan \psi = \frac{1}{x}. \quad (34)$$

The inequality $x < \cot \theta$, i.e.,

$$V_{\text{impl}} > U \tan \theta, \quad (35)$$

must also be satisfied in order for the gas to be able to impact on the projectile surface before it recedes.

Now we can set $\psi \approx \pi/2$ in case 1 of Equation 33, since $V_{\text{impl}} > \text{few } U$ for most systems of interest. With this replacement the plot of ϵ_{prop} as a function of x has two forms, as shown schematically in Figure 8, depending on whether β is $<$ or > 1 .

For cases in which $\beta < 1$, the efficiency ϵ_{prop} has a maximum value which follows from (32) as

$$\epsilon_{\text{prop}}(\text{max}) = 1 - (1 - \beta^2)^{\frac{1}{2}}, \quad (36)$$

and occurs at

$$x_M = \frac{1}{\sqrt{2}} \left(\frac{1}{\sqrt{1 - \beta^2}} - 1 \right)^{\frac{1}{2}}. \quad (37)$$

The principal matching requirement between modules and projectile needed to maintain efficient acceleration along the device is thus to match the implosion velocity so that $V_{\text{impl}} = U/x_M$, provided also that (35) is satisfied. For example, for an implosion drive situation (or mixed drive) in which half the incident kinetic energy is lost i.e., $\alpha = 0.5$, and for $\theta = \pi/4$, we find $\epsilon_{\text{prop}}(\text{max}) \approx (0.25 \text{ to } 0.12) [1 + (dM/dm)]$, and occurs at $V_{\text{impl}} \approx \text{a few times } U$.

Note also that in the ablation drive limit $V_{\text{impl}} \gg U$, $(dM/dm)_{\text{abl}} \gg 1$, case 2 of Equation 33, we recover the familiar rocket equation result

$$U = V_{\text{emiss}} \sin \theta \ln (M_i/M_f).$$

IV. PROJECTILE STABILITY, SHAPE, AND IMPLOSION REQUIREMENTS

Various tapered projectile shapes (see Figure 3) can be chosen subject to the requirements that a forward force results when the discharge implodes against its surface, and that a stable progression of the projectile occurs as it advances from module to module along the accelerator. The projectile must be stable both against tumbling and against cumulative radial drift perpendicular to the accelerator axis.

To avoid tumbling it is important for the center of mass of the projectile to be located back behind the center of thrust of the propelling force. This can be accomplished by, for example, hollowing the projectile nose or adding a slightly extended tail section as shown in Figure 3. Such a tail section could also serve to provide the trailing section of the discharge with a hard core so that kink instability cannot occur as the main tapered section advances into the next electrode gap (although since the magnetic fields are weak at impact, kinking is not expected to be a problem). Small thick fins or grooves in the trailing section could also be used for spin.

For accelerators consisting of a large number of modules it will also be necessary to ensure that the projectile does not deviate appreciably from the accelerator axis in the radial direction. In Figure 9 we show an annular implosion converging on to a cylindrical projectile which has become displaced a distance dr_{\perp} from the implosion axis. The total perpendicular momentum incident on a unit length of the projectile is thus

$$dP_{\perp} = \frac{1}{2\pi} \int_0^{2\pi} d\theta \{dr_{\perp} (1 + \sin\theta) \frac{dP}{da} - P(a)\} \sin\theta ,$$

where $P/2\pi$ is the radially directed momentum per radian of the plasma

annulus (as in Eq. (5)). If we assume that the re-emitted radial momentum per radian is an increasing function of the incident momentum, the requirement for stability against small displacements is that

$$\frac{dP_{\perp}}{dr_{\perp}} = \left(\frac{1}{2} \frac{dP}{da} \right)_{a = a_p} < 0 ,$$

i.e.,

$$\left(\frac{dP}{da} \right)_{a_p} < 0 \quad (38)$$

as shown in Figure 10 (note P is negative). Under these circumstances the side of the projectile farthest from the axis experiences a stronger impact than the side closer to the axis, so that the projectile experiences a radial "impulse well" as it advances along the accelerator. The radial shape of this impulse well for finite amplitude displacements, and assuming various models for $P(a)$, has been analyzed by T. G. Northrop.

In going from equation (4) to (9) we assumed that the annular shell thickness, Δa , was sufficiently small that the thermal pressure term could be neglected. However, this term becomes important near the end of the implosion so that (9) should more precisely be written

$$m_g \frac{d}{dt} \left[\left(1 - \frac{a^2}{a_w^2} \right) \dot{a} \right] = - \frac{I^2 \ell}{ac^2} + 2\pi \ell \int_0^{a_w} dr p . \quad (39)$$

Thus, if we arrange for the current I to become approximately zero at impact (which was the numerical example discussed in Section 2D), we see that the thermal pressure term remains in (39) and causes a deceleration just prior to impact, thereby satisfying the stability requirement (38) (see Figure 10).

Finally, we note that other approaches to stability are also possible for long multiple module devices. For example, radially offset corrector modules could be spaced at intervals along the accelerator and provide the required re-centering impulses, as computed by a logical circuit from sensor input determining the trajectory of the projectile, in which case matched implosions might not be necessary.

V. CONCLUDING COMMENTS AND APPLICATIONS

Development of the accelerator technology described here appears to have the advantage that in its initial stage it could be experimentally explored on a fairly small scale (first using a single module and kilovolt capacitors with a few kilojoules). Parameters influencing implosion stability and reproducibility, timing, the dynamic material properties of projectiles, ablation, possible multiple module implosion merging and smoothing, etc., are examples of the areas expected to play an important role in attempting to develop long length accelerators.

A fairly wide range of accelerator sizes are conceivable, depending on the applications intended. These range from basic impact studies or switching, to more advanced concepts involving mass accelerators. For example, large projectiles (kilograms) could be accelerated up to velocities of about 20 km/sec and launched as space probes through the atmosphere from a high altitude site directly into earth orbit or into space (also perhaps for radioactive waste removal). For such purposes a projectile which is both compatible with the accelerator (CM behind the center of thrust) and with aerodynamic requirements (CM ahead of center of drag) must be devised, such as the two-component projectile shown in Figure 11a.

A second potential application, this time involving projectiles of relatively small mass, is impact fusion.³ This, however, requires very long

accelerators (several 100 meters) since high velocities in the 100 km/sec range may be required. It is interesting to note that for ignition of a spherical thermonuclear pellet the outer shell must be driven inward (for example with a laser pulse) with an implosion velocity of about 200 km/sec. The radius over which these implosion velocities can be reached is limited by Rayleigh Taylor instability for large aspect ratio hollow pellets. One could view a conical plug of fusion fuel embedded in the nose of a projectile accelerated in a mass accelerator as a tamped segment of such a thermonuclear pellet, in which the fuel is driven inward with the required velocity upon impact with a target plate (Figure 11b). Rayleigh Taylor instability is avoided as the "outer shell" velocity relative to the fuel is built up in the accelerator, because the projectile and target plate remain solid prior to impact. Simple models indicate that large projectile kinetic energies (> 10 MJ) would be required for ignition in this particular arrangement due to the limited compressions attainable in such conical implosions. However, the potential advantages of impact fusion are that large total ignition energies appear to be accessible with high accelerator efficiency, and that the final transport, aiming, focussing, and small entrance hole requirements in the reactor vessel (which for example present difficulties for particle beam ignitors) are eliminated.

Note also that considerable gains occur if ignition could be achieved at lower impact velocities, through for example the use of more complex velocity multiplying projectile or target structures such as those investigated by Kaliski's⁵ group ($\sim 3 \cdot 10^7$ DD neutrons have been produced by purely chemical explosive means in these experiments). The accelerator length scales as U^2 , so that for a given projectile kinetic energy a heavier projectile ($\gtrsim 10$ gm) could be used at lower velocities, which is also needed in order to survive

the estimated ~ 0.1 cm of surface projectile ablation that would occur in an accelerator in the 100 m length range.

ACKNOWLEDGMENTS

We have enjoyed useful discussions with several colleagues, including Dr. R. Hubbard who programmed equations (17) and (18), Dr. T. G. Northrop of the Goddard Space Flight Center who carried out more detailed calculations on trajectory stability than those reported here, and Dr. P. Turchi of the Naval Research Laboratory. We are also grateful to Drs. R. A. Marshall of Texas University and Dr. Peter Kemmey of ARRADCOM for background information on mass accelerators and encouraging discussions.

REFERENCES

1. N. A. Krall and A. W. Trivelpiece, Principles of Plasma Physics, McGraw-Hill, 1973.
2. David Mosher, Coupling of Imploding-Plasma Loads to High-Power Generators, Naval Research Laboratory Report 3687, January 1978.
3. D. A. Tidman and S. A. Goldstein, Mass Accelerator for Producing Hypervelocity Projectiles using a Series of Imploded Annular Discharges, JAYCOR Tech Note 350-79-004, May 1979; to appear in Proceedings of the Impact Fusion Workshop, Los Alamos Laboratory, July 10-13, 1979; sponsored by the U. S. Department of Energy. This Proceedings contains extensive references to the Mass Accelerator literature.
4. C. Breton, C. DeMichelis, and M. Mattioli, J. Quant. Spectrosc. Radiation Transfer, 19, (1978), 367.
5. John Marshall, "Kaliski's Explosive Driven Fusion Experiments"; to appear in Proceedings of the Impact Fusion Workshop, Los Alamos Laboratory, July 10-13, 1979; sponsored by the U. S. Department of Energy. This paper contains a list of references and discussion of this work.

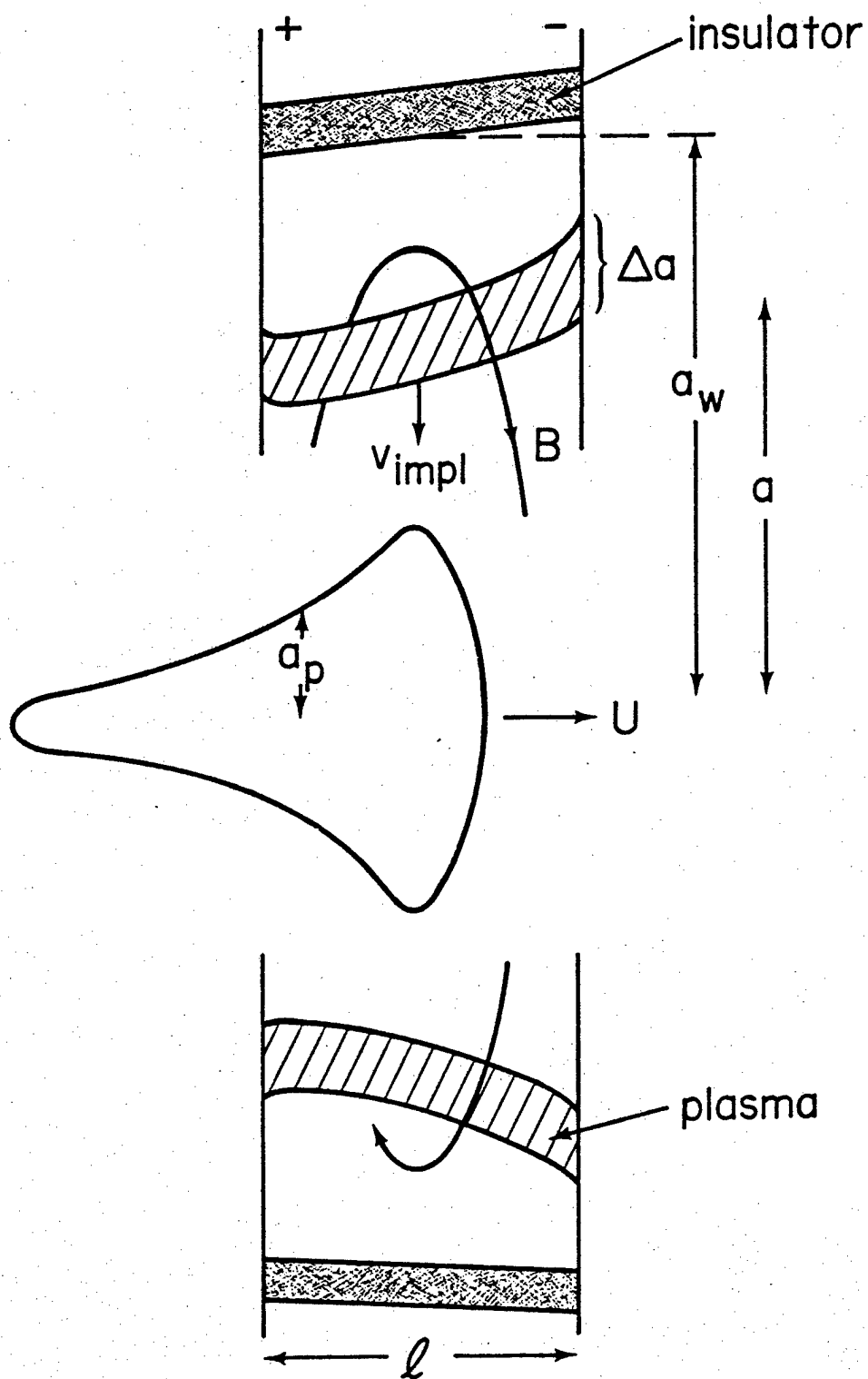


Figure 1

Annular discharge module with a driving voltage in the 1 to tens of kilovolts range. Power compression occurs when the plasma implosion time is longer than the projectile transit time through the module. This particular module is shown with a slight insulator tilt to produce tapered implosions. The simpler straight insulator system is shown in Figure 2.

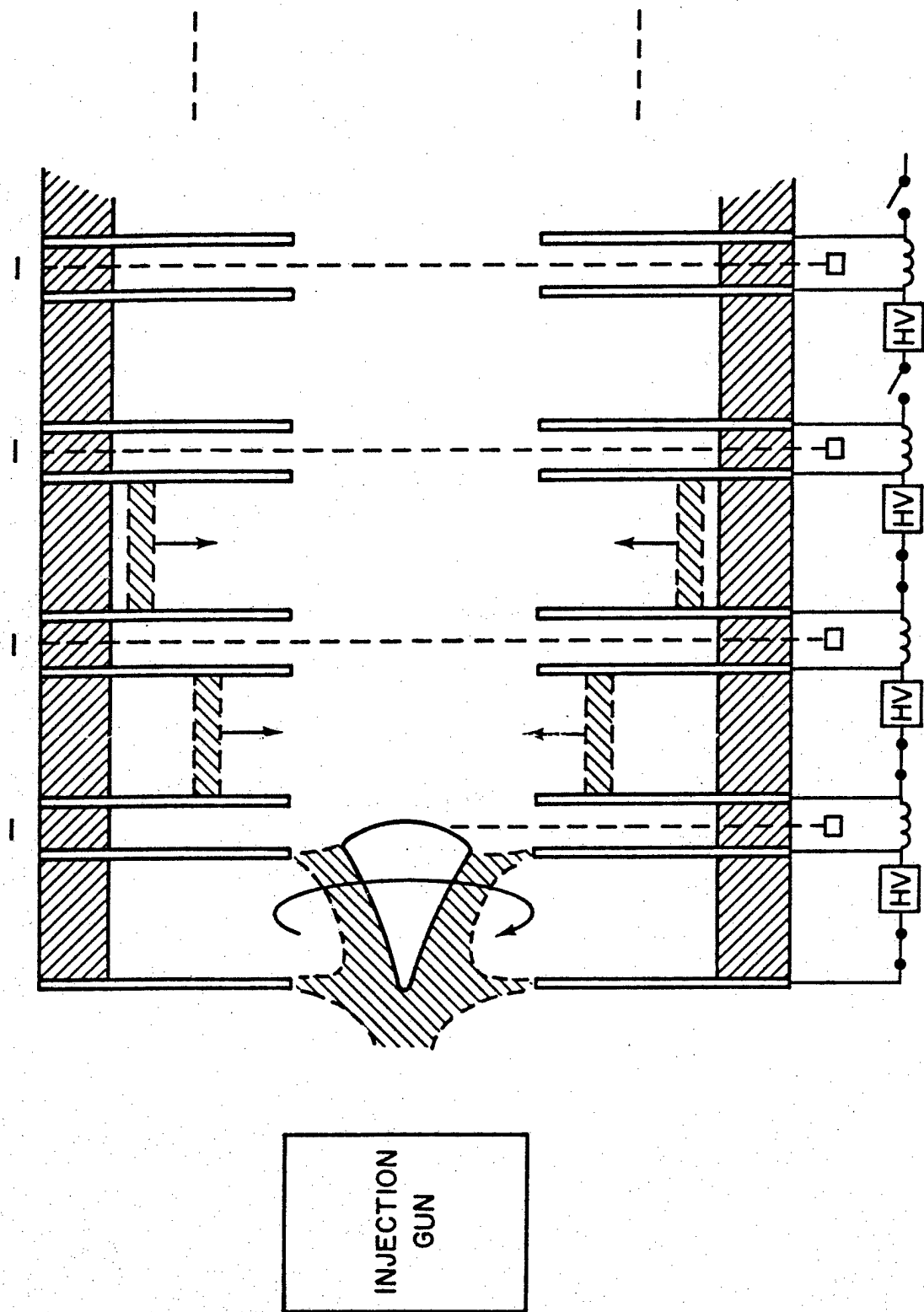


Figure 2

Mass accelerator using imploded discharges (MAID). Assuming the gas mass m_g in the accelerator is sequentially swept up and imploded with velocity V_{imp1} against a projectile of cone half angle θ and mass M , the simple specular reflection limit gives $U \sim m_g V_{imp1} \sin 2\theta / M$ for the final projectile velocity. For more general cases including the ablated mass reaction see Section III. More closely packed multiple module systems can also be designed.³

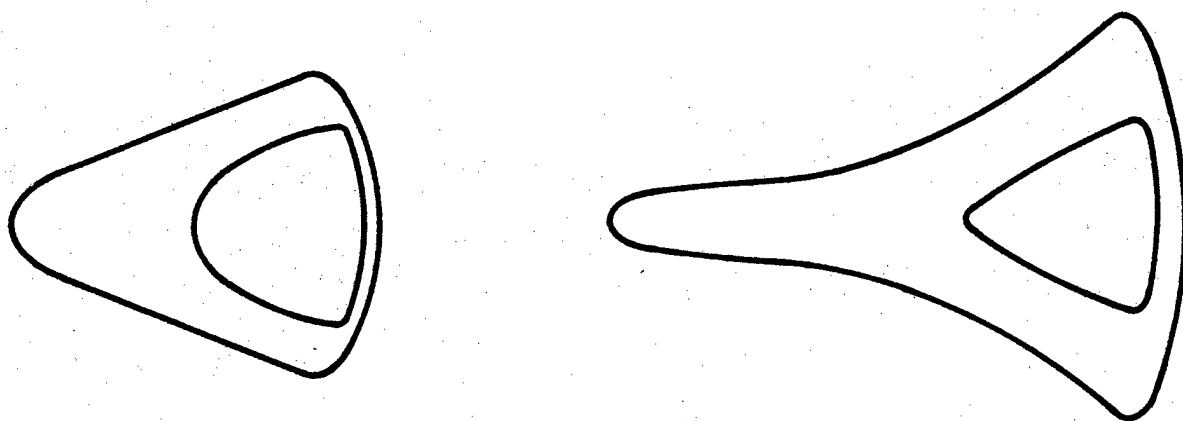


Figure 3

Projectiles of either metal or insulator with nose cavities which serve to move the center of mass back behind the center of thrust in the accelerator for stability. Small thick oblique tail fins or grooves could also be used to spin the projectile if needed. Inner structures can also be designed to minimize shock convergence onto the projectile axis.

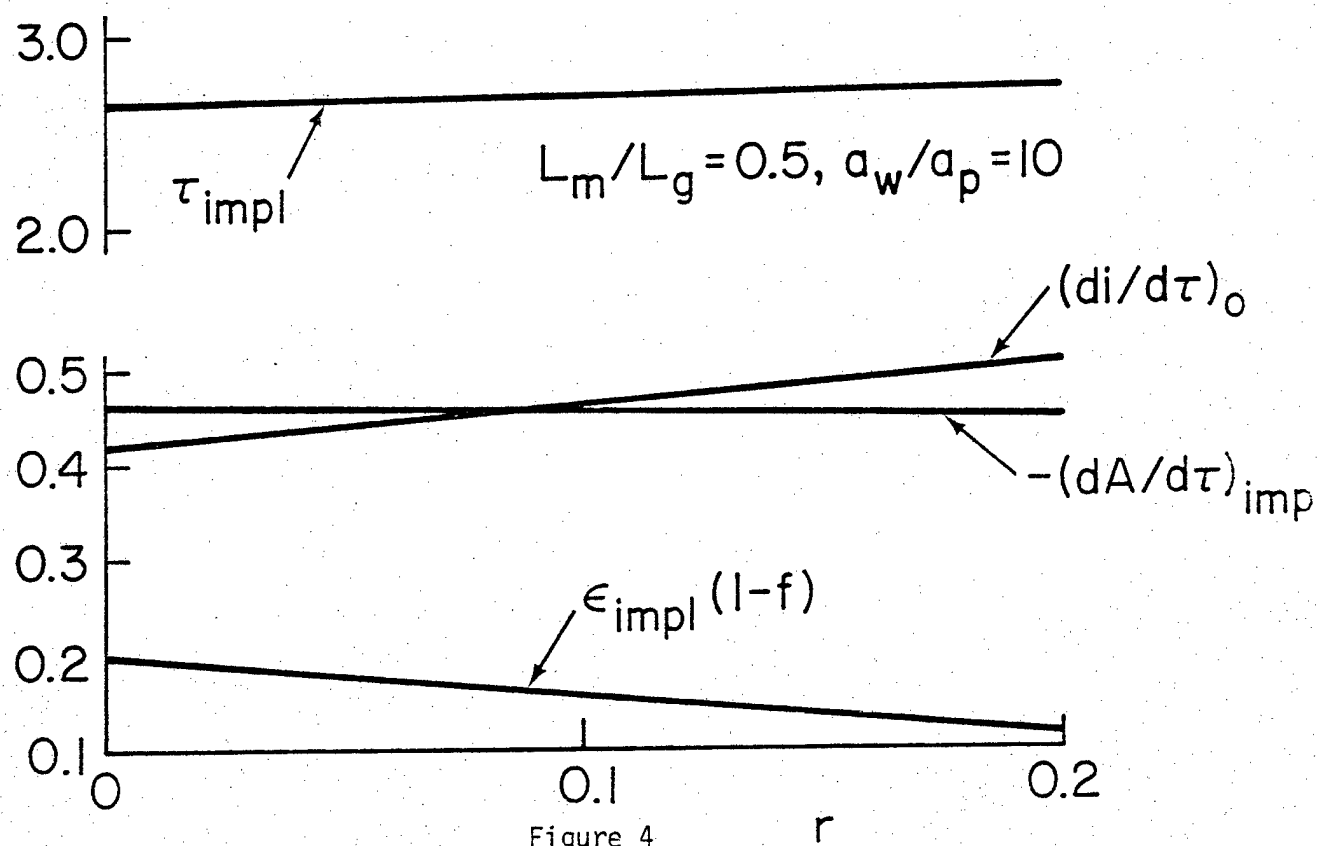
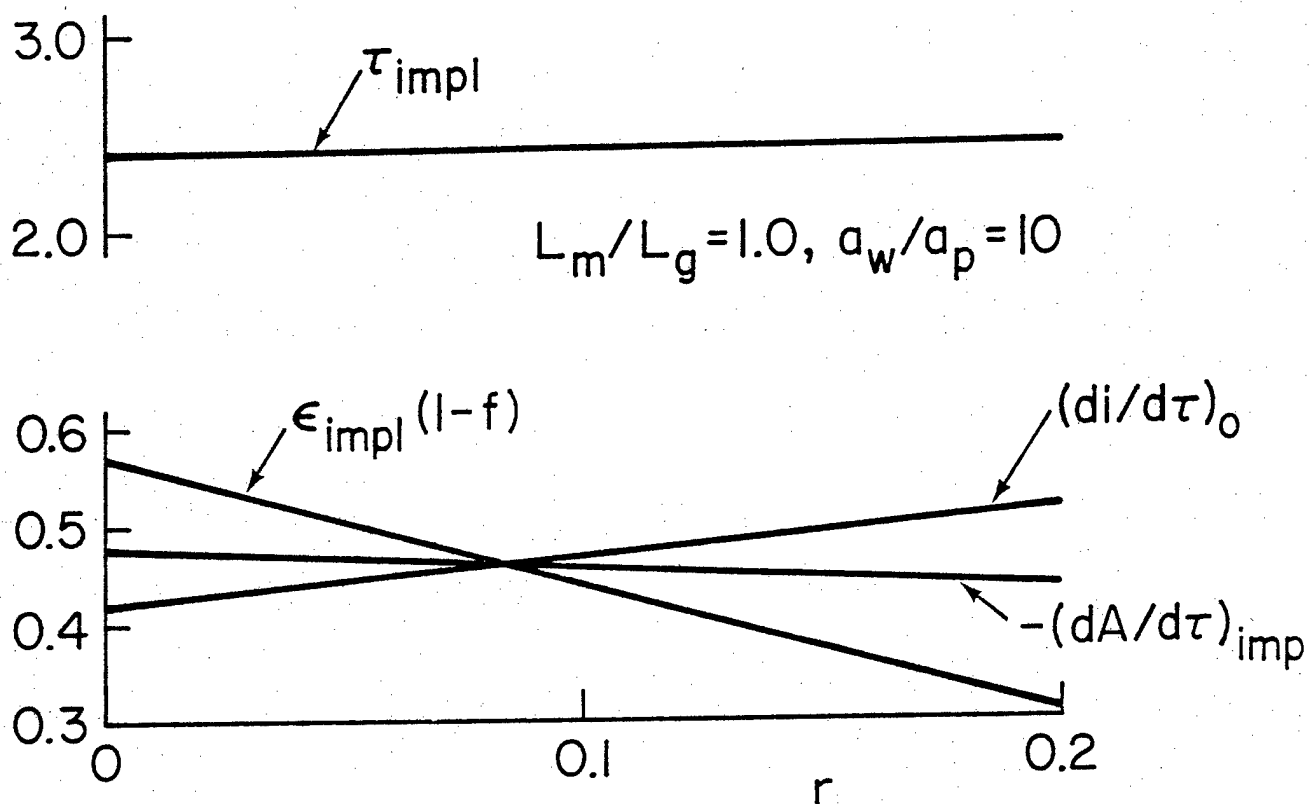


Figure 4

Plots of the dimensionless impact velocity, $(dA/d\tau)_{imp}$, plasma implosion time τ_{impl} , initial current gradient $(di/d\tau)_0$, and implosion efficiency, for two matched cases (i.e., cases for which the current at impact is zero) as functions of $r = 2\ell/ca_w L_0 (4\pi\sigma\omega)^{1/2}$. Higher efficiencies than the above simple circuit model cases (Eqs. 10,18) may be achievable by use of pulse forming transmission lines to reduce the wave reflected from the module back into the capacitor.

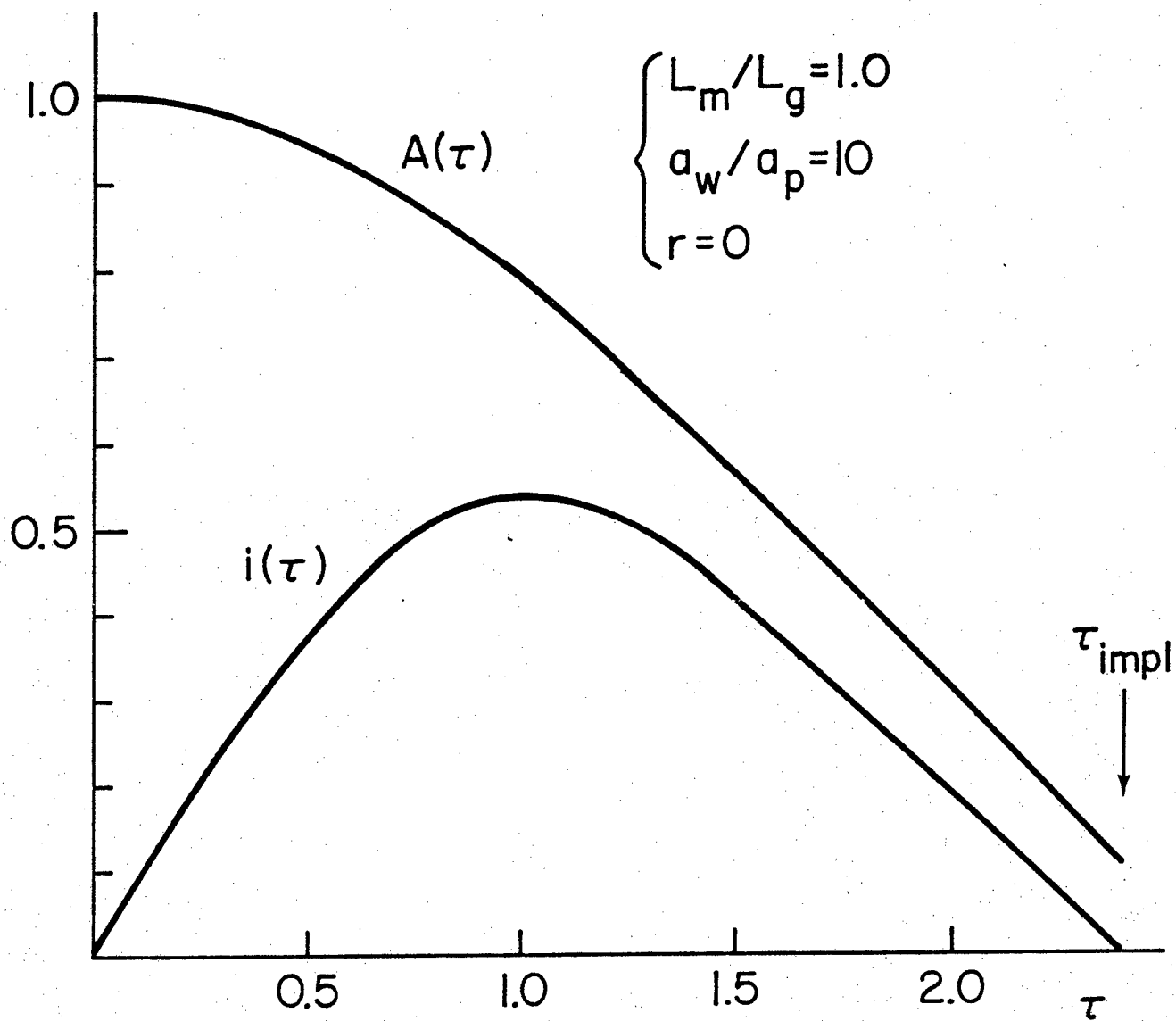


Figure 5

Plot of the dimensionless radius $A = a/a_w$ and current $i = I/I_0$ as a function of $\tau = \omega t$ for an implosion in which electrical resistance of the discharge is neglected.

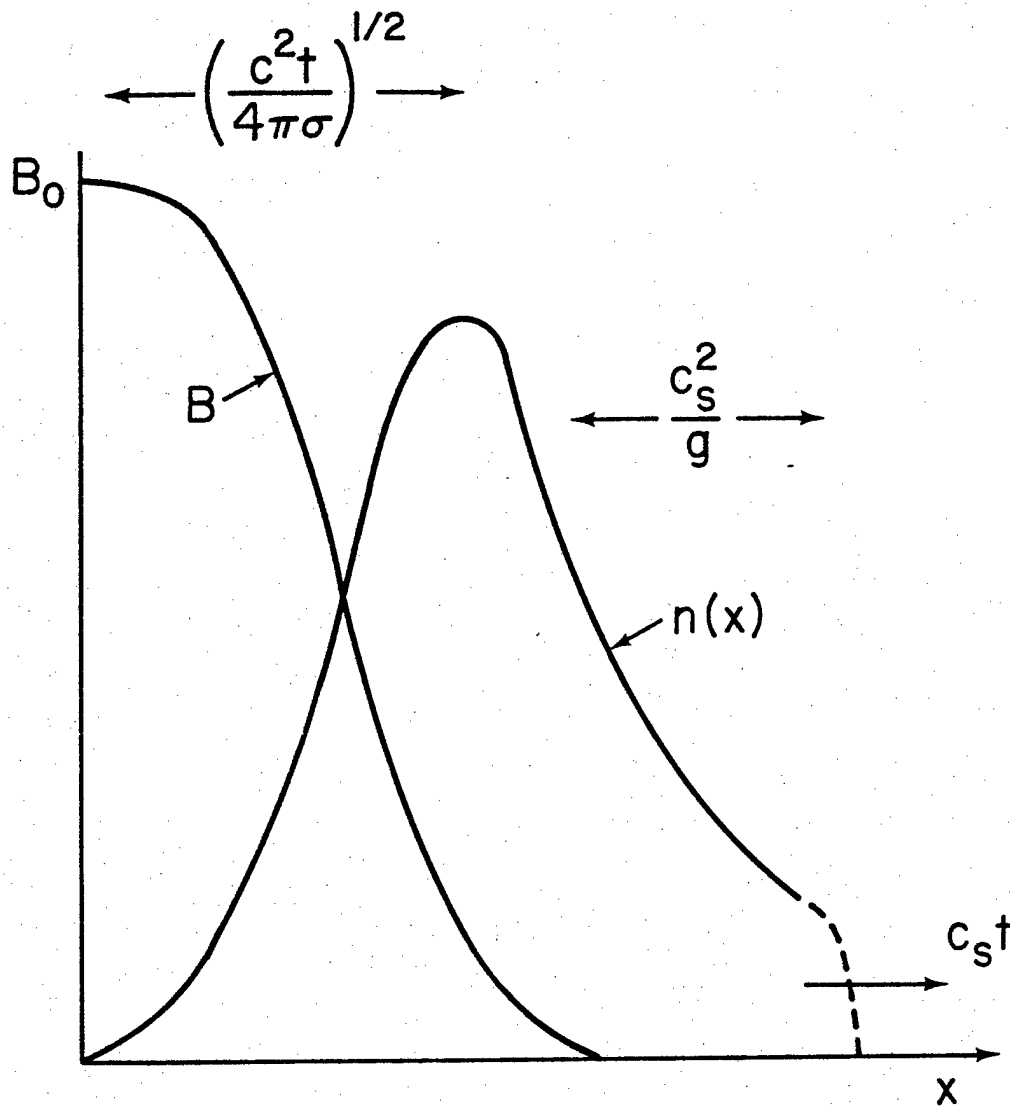


Figure 6

Schematic plot of the variation of plasma density n and magnetic field for a layer of plasma undergoing an acceleration g .

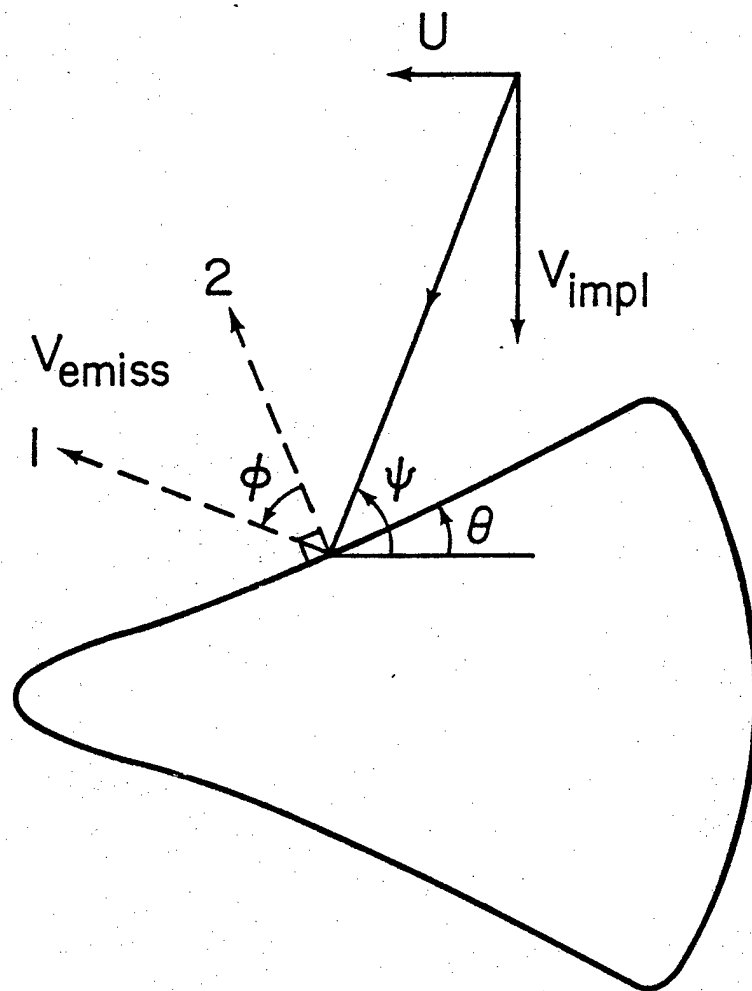


Figure 7

Collision of imploding plasma with the projectile surface in the projectile rest frame.

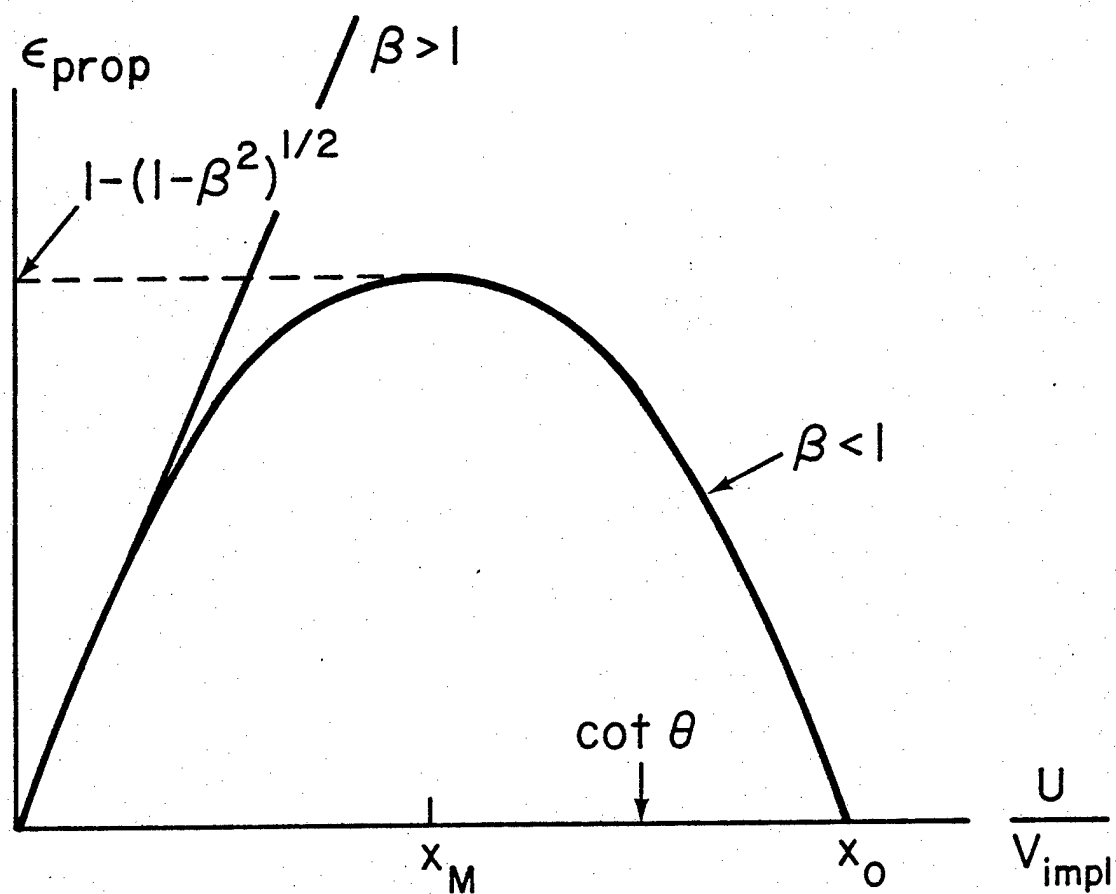


Figure 8

Variation of the propulsion efficiency, ϵ_{prop} (Equation 32), with U/V_{impl} .

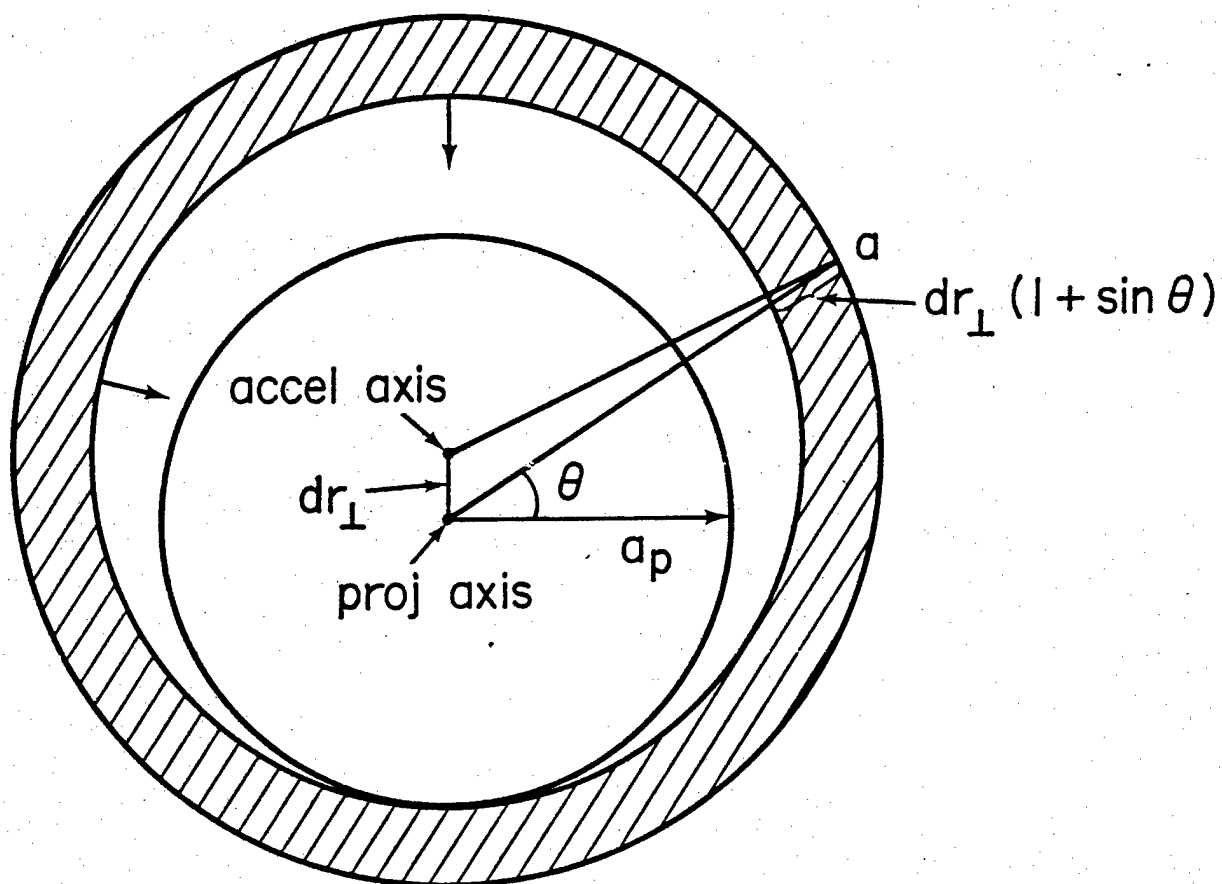


Figure 9

Impact of imploding plasma annulus with a projectile that has become displaced a distance dr_{\perp} from the accelerator axis.

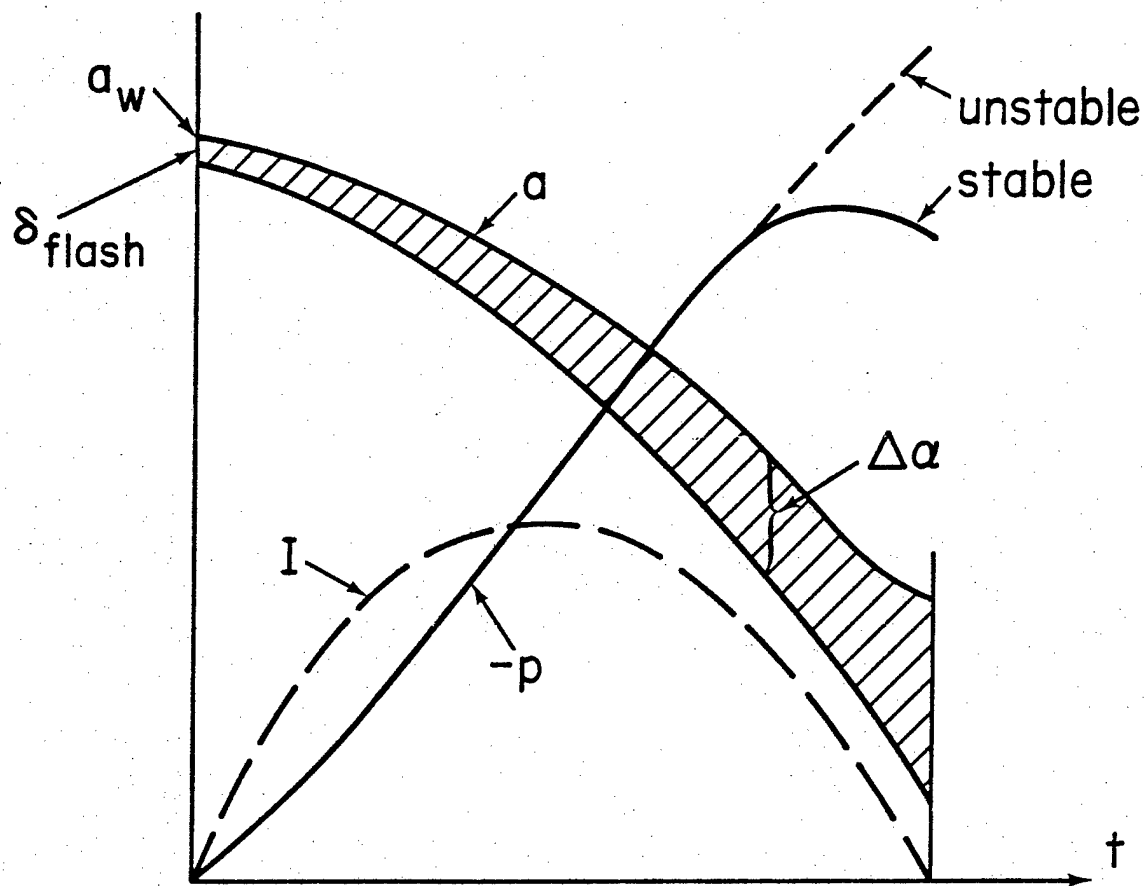


Figure 10

A matched implosion, $i(\tau_{imp}) = 0$, showing the final decrease in the implosion momentum due to plasma thermal pressure forces as required to provide a stabilizing restoring impulse for projectile radial displacements. Although the above radially integrated momentum decreases, the inner edge of the annulus would continue to accelerate inward and the outer radial region to decelerate near the end of the implosion.

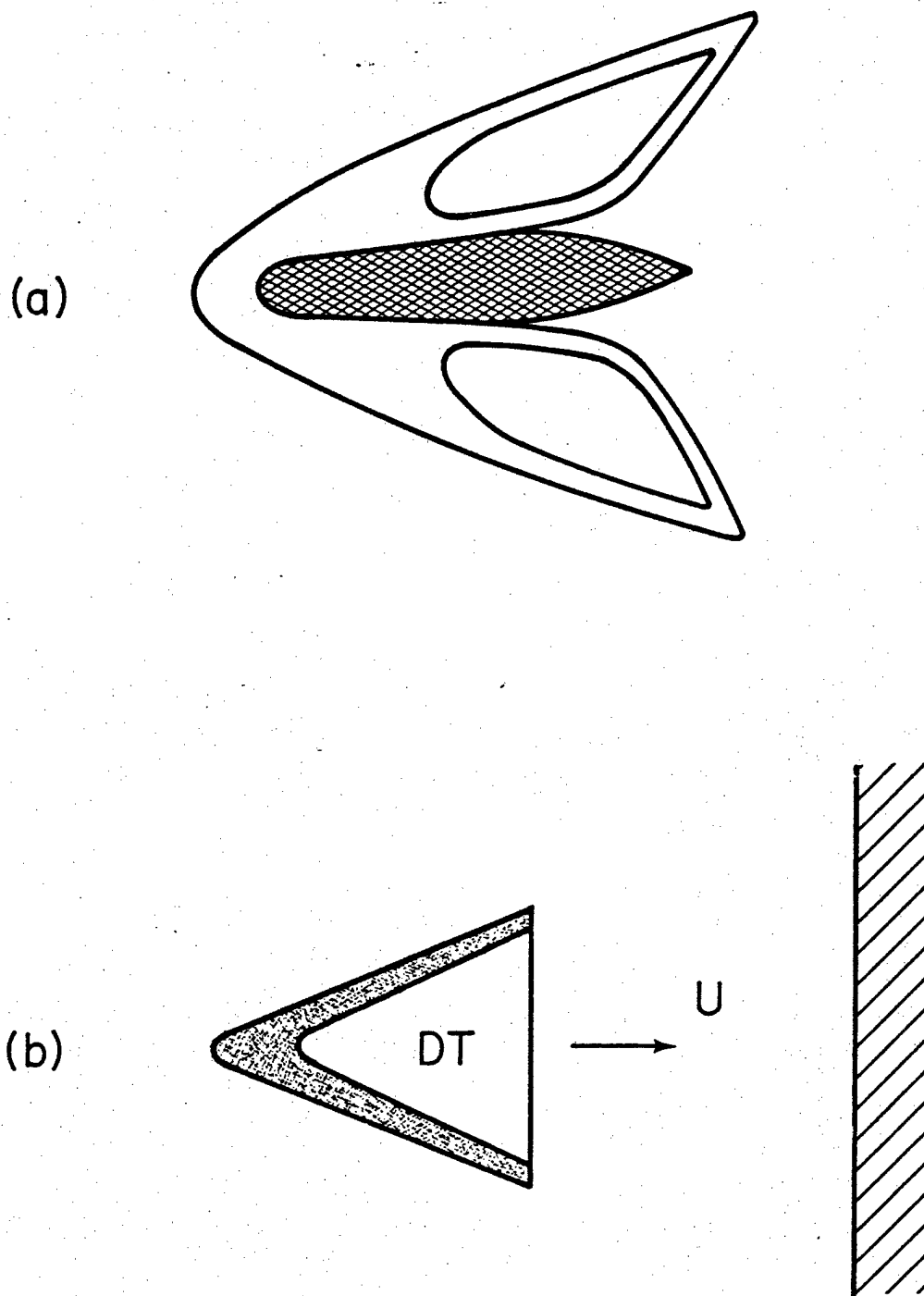


Figure 11

Two examples of complex projectile structures. Case (a) is an accelerated structure in which the outer jacket is stripped off by air resistance when it exits the accelerator and the inner aerodynamically suitable projectile proceeds on. Case (b) is an illustration of a projectile which gives rise to a tamped conical compression of DT thermonuclear fuel on impact with a target plate. More complex velocity-multiplying structures⁵ would also be possible.